Published in final edited form as:
Nat Neurosci. 2008 August ; 11(8): 901–907. doi:10.1038/nn.2156.

Neurons born in the adult dentate gyrus form functional synapses with target cells

Nicolas Toni[1,4], **Diego A Laplagne**[2,4], **Chunmei Zhao**[1], **Gabriela Lombardi**[2], **Charles E Ribak**[3], **Fred H Gage**[1], and **Alejandro F Schinder**[2]

1*Laboratory of Genetics, Salk Institute, 10010 North Torrey Pines Road, La Jolla, California 92037, USA*

2*Laboratory of Neuronal Plasticity, Leloir Institute–CONICET, Av. Patricias Argentinas 435, (1405) Buenos Aires, Argentina*

3*Department of Anatomy & Neurobiology, University of California at Irvine, School of Medicine, Irvine, California 92697-1275, USA*

Abstract

Adult neurogenesis occurs in the hippocampus and the olfactory bulb of the mammalian CNS. Recent studies have demonstrated that newborn granule cells of the adult hippocampus are postsynaptic targets of excitatory and inhibitory neurons, but evidence of synapse formation by the axons of these cells is still lacking. By combining retroviral expression of green fluorescent protein in adult-born neurons of the mouse dentate gyrus with immuno-electron microscopy, we found output synapses that were formed by labeled terminals on appropriate target cells in the CA3 area and the hilus. Furthermore, retroviral expression of channelrhodopsin-2 allowed us to light-stimulate newborn granule cells and identify postsynaptic target neurons by whole-cell recordings in acute slices. Our structural and functional evidence indicates that axons of adult-born granule cells establish synapses with hilar interneurons, mossy cells and CA3 pyramidal cells and release glutamate as their main neurotransmitter.

Increasing evidence supports the hypothesis that neurogenesis is a physiologically important event in the adult hippocampus, but the precise role of newly generated cells in the hippocampal network remains unknown[1-5]. Understanding how newborn granule cells may contribute to information processing in the adult hippocampus requires a detailed analysis of their connectivity and function. Previous studies have clearly demonstrated that newborn neurons in the adult hippocampus receive morphologically mature axo-somatic, axo-dendritic and axo-spinous synapses and that those inputs arising from the entorhinal cortex and local inhibitory interneurons are fully functional[6-13]. To influence information processing in the hippocampal network, new granule cells must also contact the appropriate neuronal targets, but this capability has not yet been demonstrated because of technical challenges.

Correspondence should be addressed to F.H.G. (gage@salk.edu) or A.F.S. (aschinder@leloir.org.ar).
[4]These authors contributed equally to this work.

AUTHOR CONTRIBUTIONS N.T. contributed to the concept, designed and carried out the structural experiments, analyzed the data, and wrote the manuscript. D.A.L. contributed to the concept, designed and performed the functional experiments, analyzed the data, and wrote the manuscript. C.Z. contributed to the experimental design, provided samples for the structural experiments, carried out and analyzed confocal images of presynaptic terminals, and revised the manuscript. G.L. prepared retroviral stocks, performed immunofluorescence and obtained images of ChR2-positive neurons. C.E.R. contributed to setting up the technique for immuno-electron microscopy of GFP, the analysis of electron micrographs, and the writing and revision of the manuscript. F.H.G. and A.F.S. contributed to the concept, designed the experiments, analyzed the data, wrote the manuscript and provided financial support.

Published online at http://www.nature.com/natureneuroscience/

In this study, we searched for structural and functional evidence for output synapses of adult-born granule cells. Mossy fibers, the axons of granule cells, are known to contact inhibitory interneurons of the granule cell layer (GCL), hilus and CA3 area as well as excitatory mossy cells in the hilus and CA3 pyramidal cells[14]. We used retroviral expression of the green fluorescent protein (GFP) to identify newly generated neurons[15] and carried out immuno-electron microscopy of labeled cells. We found axo-dendritic and axo-spinous synapses that were formed by labeled terminals with hilar interneurons and CA3 neurons. Those contacts started to form by the third week of neuronal development, even before newborn cells had reached complete maturation. To determine whether these synapses are functional, we expressed the light-gated cation channel channelrhodopsin-2 (ChR2) in the progeny of dividing neural precursors of the adult dentate gyrus. Postsynaptic responses evoked by light stimulation of newborn granule cells were then recorded in acute hippocampal slices. We found that axons of newborn neurons released glutamate onto a variety of postsynaptic neuronal targets in the dentate gyrus.

RESULTS

Injections of the retroviral vector CAG-GFP into the dentate gyrus of 6-to 7-week-old mice resulted in the labeling of newly generated granule cells with GFP[6,15]. We observed axons and axon terminals in the hilus and the CA3 areas using confocal microscopy. We found that the mossy fiber boutons in CA3 were substantially larger at 28 and 75 days post viral injection (dpi) than those at 17 dpi (Fig. 1). At later time points, the mossy fiber boutons had long extensions, as previously described[16]. The size of the GFP-labeled mossy fiber boutons at 75 dpi was similar to that of the mature neurons born during early postnatal development ((P = 0.18) Fig. 1b,c,d,f). Notably, the size of the mossy fiber boutons in the hilus did not change significantly during the maturation of newborn neurons (P = 0.65). Furthermore, the average size of the mossy fiber boutons in CA3 was significantly larger than that in the hilus ($P < 0.001$, Student's t test), except for new neurons at 17 dpi.

We then used immuno-electron microscopy for GFP and serial-sectioning to analyze boutons that were formed by labeled axons. A total of 44 axonal boutons were sectioned, all of which formed synapses on either CA3 or hilar neurons (Fig. 2). We found synapses on thorny excrescences, dendritic spines or dendrites, which were unambiguously identified by the presence of at least four presynaptic vesicles within 100 nm of the active zone, a well-defined synaptic cleft, and postsynaptic density. We observed large mossy terminals synapsing with thorny excrescences (Fig. 2a,b) as well as boutons synapsing with spiny dendrites in the CA3 area (Fig. 2c) and with thorny excrescences in the hilus (Fig. 2). In addition, the thin GFP-positive axons (~0.1 to 0.2 μm in diameter) also formed *en passant* synapses with thin dendritic shafts at each of the time points in both CA3 and the hilus (Fig. 2d,e). In our serial sections, these thin dendrites were aspiny, suggesting that they arose from GABAergic interneurons[17]. These aspiny dendrites were postsynaptic to both the GFP-positive axons and other thin axons that lacked GFP (Fig. 2d,e). Furthermore, there were no intervening glial processes between the thin GFP-positive axons and the unlabeled axons. Further evidence of newborn granule cells forming synapses with GABAergic interneurons is provided below. Thin GFP-positive axons also synapsed onto the spines of thin dendrites, probably arising from spiny interneurons located in the stratum lucidum of CA3 (ref. 18).

We next examined the connectivity of GFP-positive mossy fibers that synapsed with dendrites of CA3 pyramidal cells (Fig. 3). At 17 dpi, 6 out of 8 GFP-positive mossy fiber boutons had formed synapses with the dendritic shafts of pyramidal cells (Fig. 3a,b), whereas adjacent thorny excrescences and their spines[19] were contacted by large, unlabeled mossy fiber boutons. The other two GFP-positive boutons at 17 dpi synapsed onto thorny excrescences that were shared with GFP-negative boutons. At 28 dpi, 10 out of 11 GFP-positive mossy fiber boutons

shared both the thorny excrescence and spines with one or two GFP-negative mossy fiber boutons (Figs. 2a and 3c,d), whereas one bouton had synapsed directly with the dendritic shaft of a pyramidal neuron. At 75 dpi, 10 out of 12 GFP-positive mossy fiber boutons were entirely associated with one individual thorny excrescence with spines, and this synaptic complex was enveloped by astrocytic processes (Fig. 3e,f). The other two boutons shared a spine with a GFP-negative terminal.

The number of spines enveloped by each GFP-positive mossy fiber bouton increased significantly from 0.1 at 17 dpi ($n = 7$) to 2 at 28 dpi ($n = 9$) and 3.8 at 75 dpi ($n = 10$) (17 versus 27 dpi, $P<0.05$; 28 versus 75 dpi, $P < 0.05$). In comparison, there were 2.9 spines per GFP-negative bouton ($n = 11$; Fig. 3g). The total cross-sectional area of GFP-positive mossy fiber boutons also substantially increased over this time period, with the greatest increase occurring between 17 and 28 dpi (Fig. 3h). Although some of the presynaptic vesicles were obscured by the immunostaining for GFP, which resulted in an underestimation of their total number, we found a significant increase in presynaptic vesicles from 60 at 17 dpi to 120 at 28 dpi, 179 at 75 dpi and 240 in GFP-negative boutons (17 versus 75 dpi, $P < 0.05$; 75 dip versus GFP negative, $P < 0.005$; Fig. 3i). Large dense-core and large clear-core vesicles were also present at all of the time points examined. The number of active zones also increased from 3 at 17 dpi to between 5 and 6 at 75 dpi and in GFP-negative boutons (17 versus 75 dpi, $P < 0.05$; Fig. 3j). A model for the maturation of axonal boutons is shown in Supplementary Figure 1 online.

We then investigated whether the output synapses formed by newly generated neurons are functional. The most direct approach would involve double patch recordings of presynaptic GFP-positive cells connected to target neurons in acute brain slices. However, such paired recordings are technically challenging, as each cell only contacts a small fraction of all possible targets[20,21] and axons may be severed during slice preparation. To overcome this problem, we developed a retroviral vector carrying ChR2 (refs. 22,[23]) and a fluorescent reporter gene (GFP or monomeric red fluorescent protein 1, mRFP1) with which to transduce the progeny of dividing progenitor cells of the dentate gyrus of adult mice. In these conditions, large populations of adult-born granule cells could be readily activated by blue light in acute hippocampal slices (Supplementary Fig. 2 online). Thus, ChR2 can now be used to evoke neurotransmitter release from the mossy fiber terminals of a large population of adult-born granule cells to find connected target neurons using whole-cell patch-clamp recordings.

To determine whether new neurons establish functional synapses with their targets, we used brain slices (3–4 months after retroviral labeling) containing several dozen fluorescent cells to assess responses to light-driven mossy fiber stimulation in randomly selected putative postsynaptic cells. Cellular targets of mossy fibers are distributed in the hilus, GCL/hilar border and CA3 region, and include GABAergic interneurons, mossy cells and pyramidal neurons[21]. We carried out whole-cell recordings in randomly selected neurons of these areas and determined their identity by considering electrophysiological and anatomical parameters, including location of the soma, morphology, firing properties and spontaneous synaptic activity (Supplementary Methods, Supplementary Fig. 3 and Supplementary Table 1 online). Briefly, interneurons are located in the hilus and the GCL/hilar border, spike with high frequency and have a pronounced afterhyperpolarization (AHP); mossy cells are located in the hilus, reach lower firing frequencies, lack AHP and show a high frequency of spontaneous synaptic activity; and pyramidal cells are found in the CA3 pyramidal layer and display intermediate spiking and AHP properties.

We tested light-induced postsynaptic responsiveness in 107 putative target cells that included 76 interneurons, 16 mossy cells, 11 pyramidal cells and 4 unclassified neurons (Fig. 4, an example of a successful recording obtained from a cell identified as a GABAergic interneuron

of the GCL/hilar border is shown in Fig. 4a–e). Prolonged light stimulation of the slice elicited a high frequency of inward synaptic currents (Fig. 4c). Repetitive light pulses of short duration delivered at low frequency (10 ms, 0.2 Hz) elicited postsynaptic currents (PSCs) that were time-locked to the stimulus (Fig. 4d,e). For each cell, we averaged tens to hundreds of stimuli presentations to distinguish light-evoked PSCs from uncorrelated spontaneous activity (Fig. 4k,l). PSCs were successfully evoked in 14 target cells (Fig. 4p) that corresponded to GABAergic interneurons (n = 11; two examples in Fig. 4a–e and Fig. 4f–i), one mossy cell (Fig. 4j–l), one CA3 pyramidal cell (Fig. 4m–o) and one unclassified neuron.

Light-evoked synaptic responses should be subject to blockade by the appropriate receptor antagonists. Mossy fiber stimulation should typically evoke glutamatergic responses, although other possibilities have also been proposed, especially in developing neurons or after seizures[24,25]. Polysynaptic inhibitory and excitatory signals can also be observed if mossy fiber activation recruits local interneurons or mossy or pyramidal cells, respectively[26-28]. Both types of responses ultimately depend on glutamate release from mossy fibers and should therefore be blocked by the mixed AMPA/NMDA receptor antagonist kynurenic acid (Kyn, 4–10 mM). Light-evoked responses of adult-born neurons showed a pharmacological profile that was consistent with this notion, as Kyn consistently abolished evoked PSCs in a reversible manner (Fig. 5). The metabotropic GluR agonist DCG-IV, which reduces neurotransmitter release at mossy fiber terminals[29], also blocked PSCs (example shown in Fig. 5a,b; similar results were obtained in two experiments).

We also tested the effect of the $GABA_A$ receptor antagonist bicuculline methiodide (BMI, 20 μM) to identify putative feedforward inhibition. In 3 out of 5 cases, BMI elicited little or no changes in PSC amplitude, whereas subsequent addition of Kyn completely abolished the responses, confirming their glutamatergic nature (Fig. 5c,d,f). In the remaining two cases, BMI blocked a substantial proportion of the PSC, but complete block was also observed in the presence of Kyn, consistent with feedforward GABAergic inhibition that is dependent on glutamate release from mossy fiber terminals (Fig. 5e,f).

DISCUSSION

It has been recently demonstrated that newborn granule cells of the adult hippocampus receive functional synaptic inputs that can drive them to spike[6-13]. Our study demonstrates that newborn neurons can also influence the activity of the downstream network, as both structural and functional properties of their synaptic terminals are compatible with a full integration into hippocampal circuitry.

At the structural level, we found that axons arising from adult-generated granule cells made synapses with postsynaptic targets in the CA3 area and the hilus as early as 17 d after cell division and that these synapses continued to mature thereafter. At first, axonal boutons synapsed with dendritic shafts of postsynaptic targets and then contacted spines, or thorny excrescences, a time course that is consistent with data from studies of hippocampal development[30,31]. In contrast with these studies, however, newly generated neurons had intermediate stages where they synapsed with thorny excrescences that were also contacted by GFP-negative neurons. This observation raises the possibility that the development of mossy fiber synapses from newly generated neurons involves the recruitment of pre-existing postsynaptic targets, where boutons may compete for thorny excrescences in a fashion similar to that observed during the development of their dendritic spines[12] (Supplementary Fig. 1). Notably, the time course of mossy terminal maturation appears to be concurrent with dendritic spine maturation on GFP-positive neurons[12,13,15], suggesting that the functional input and output of newborn neurons is synchronized and occurs in a discrete time frame. Finally, our structural data strongly suggest that mossy fibers make contacts with interneurons of the hilus

and the GCL/hilar border. This observation was confirmed by our functional studies, in which the identity of postsynaptic neurons was unambiguously determined using electrophysiological and anatomical parameters (Supplementary Fig. 3 and Supplementary Table 1).

Restricted expression of ChR2 served to specifically stimulate large groups of adult-born granule cells at mature stages and detect neurotransmitter release onto target cells as postsynaptic responses that were time-locked to the stimulus (Fig. 4). Together with the morphological profile described above, these observations demonstrate that contacts formed by newborn granule cells onto target neurons are functional glutamatergic synapses (Fig. 5).

Light-evoked PSCs may reflect a direct contact between a mossy fiber terminal and a recorded cell (monosynaptic connection; see scheme in Supplementary Fig. 4 online) or an indirect pathway involving the activation of intermediary neurons (polysynaptic connection; Supplementary Fig. 4). Detailed analysis of postsynaptic responses indicated that 7 out of 14 recordings probably correspond to monosynaptic responses, whereas two were mediated by GABAergic interneurons (see Methods; the remaining five neurons could not be reliably classified). The observation of these polysynaptic responses indicates that newborn granule cells can trigger spiking of postsynaptic neurons.

Our present findings demonstrate that axons of newborn cells establish synaptic connections with mossy cells, interneurons of the hilus and GCL/hilar border, and pyramidal cells, and release glutamate as the main neurotransmitter. New neurons are therefore fully functional units of the hippocampal circuit, being able to effectively integrate input information and transmit it to postsynaptic targets. From a global point of view, these properties are similar to those of all of the other granule cells of the adult dentate gyrus, similar to what has been reported for afferent connections[10,12,32]. However, it is conceivable that subtle differences might be present in the identity of presynaptic neurons and postsynaptic targets, or in the degree of functional plasticity of synapses formed onto[7,11,33] or by these cells.

METHODS

Animals

Female C57Bl/6 mice, 5–7 weeks old, were injected with murine leukemia–based retroviruses as described previously[10,15] and were housed with unlimited access to running wheels starting from 3–7 d before virus injection. At the indicated times post–viral injection, depending on the experimental design, mice were anesthetized with a mixture of ketamine and xylazine (100 mg per kg of body weight, 10 mg per kg) and perfused transcardially with 0.9% saline (wt/vol), followed by 4% paraformaldehyde (PFA, wt/vol). The brain samples were postfixed with 4% paraformaldehyde for an additional 2 d. We prepared 50-μm coronal sections with a vibratome. Mice destined for electrophysiological studies received a vitamin A–containing multivitamin supplement to ensure the availability of retinal precursors needed for ChR2 function. The animal protocols were approved by the Salk Institutional Animal Care and Use Committee.

Viral vectors

A replication-deficient retroviral vector based on the Moloney murine leukemia virus was used to express either GFP alone[15] or ChR2. Two ChR2 constructs were used: CAG–ChR2-GFP, expressing a ChR2-GFP fusion protein[23] driven by a CAG promoter, and PGK–ChR2-IRES-RFP, expressing a C-terminally truncated version of ChR2 (amino acids 1–315) and mRFP1 (ref. 34) driven by the phosphoglycerate kinase (PGK) promoter. Retroviral particles were assembled using three separate plasmids containing the capsid (CMV-vsvg), viral proteins (CMV-gag/pol) and transgene (CAG-GFP, CAG-ChR2 or PGK–ChR2-IRES-RFP). Plasmids were transfected onto 293T cells using Lipofectamine 2000 (Invitrogen). Virus-containing

supernatant was harvested 48 h after transfection and concentrated by two rounds of ultracentrifugation.

Confocal analysis of mossy fiber boutons

Images of GFP-labeled mossy fiber axons in the CA3 region were acquired at 0.75-μm intervals with the Bio-Rad R2100 confocal system with a plane apochromatic 40× oil lens (numerical aperture, 1.3; Nikon) and a digital zoom of 6. The Bio-Rad image files were subjected to five iterations of deconvolution with the AutoDeblur program (AutoQuant). Maximum projections of *z* series were created with the Confocal Assistance Program in BMP format and the files were then imported into IGL Trace (http://synapse-web.org/tools/index.stm). Mossy fiber boutons that fit the following criteria were selected for quantification: (i) the diameter of the bouton was more than threefold greater than the diameter of the mossy fiber, (ii) the bouton was connected to the mossy fiber on at least one end and (iii) the bouton was relatively isolated from other boutons for accuracy of tracing. These criteria were arbitrary but nevertheless established an unbiased sampling. The contour of the boutons was traced manually and the enclosed area was calculated by the IGL Trace program. A total of 20–21 boutons were analyzed for each time point in CA3 and a total of 20–66 boutons were analyzed for each time point in the hilus.

Electron microscopy

Mice were transcardially perfused with 4% PFA in 0.1 M phosphate buffer, pH 7.4, and maintained at 4 °C. We removed the brain 15 h after the perfusion was stopped and postfixed it for 72 h in 4% PFA. We then cut 50-μm horizontal vibratome sections and observed them under an epifluorescence microscope. One brain, which had an insufficient amount of labeled cells, was discarded. The sections of the remaining brains were then cryoprotected in 2% glycerol and 20% DMSO (vol/vol) in 0.1 M phosphate buffer for 20 min and freeze-thawed four times in liquid nitrogen. After a treatment in 0.3% hydrogen peroxyde (vol/vol, five times for 5 min) and three 10-min washes in 0.1 M phosphate buffer + 0.5% bovine serum albumin (vol/vol, BSA-C, Aurion), slices were incubated overnight in the primary antibody (rabbit antibody to GFP, 1:500, Chemicon) in phosphate buffer + 0.1% BSA-C for 40 h, at 4 °C on a shaker. After washing in phosphate buffer + 0.1% BSA-C, the sections were incubated for 5 h at 20 ± 5 °C in biotinylated secondary antibody (goat antibody to rabbit (F)ab fragment, 1:200, Jackson Laboratories). To reveal this labeling, we incubated slices for 2 h in avidin biotin peroxidase complex (ABC Elite, Vector Laboratories), followed by 3,3′-diaminobenzidine tetrachloride (Vector Laboratories Kit) for 10–20 min. The sections were then postfixed overnight in 2.5% glutaraldehyde (wt/vol), washed in phosphate buffer 0.1 M, postfixed in osmium tetroxide for 1 h, dehydrated in ascending concentrations of ethanol and then acetone, and embedded in Epoxy resin.

Serial sections at a depth of more than 5 μm were cut at 40-nm thickness and collected on single-slot grids, then contrasted by incubating for 35 min in 5% uranyl acetate solution (wt/vol), followed by 25 min in a Reynolds solution. Serial images of the labeled structures were then collected with a digital camera (MegaView III, SIS) mounted on a JEOL 100 CXII transmission electron microscope at a 19,000× magnification with a filament voltage of 80 kV. Serial images were then aligned and three-dimensional structures were rendered using Reconstruct 1.0 (provided by J. Fiala, Boston University).

Electrophysiology

Experiments were carried out in 43 slices from 34 mice, 14.9 ± 2.9 weeks (mean ± s.d., range: 8.6–20.6) after injection of the retrovirus. Light-evoked PSCs were detected in 14 neurons in 11 slices from 9 mice, 16.0 ± 1.9 (range: 13.4–20.4) weeks after the injection. Mice were anesthetized and decapitated. Brains were removed and placed into a chilled solution

containing 110 mM choline chloride, 2.5 mM KCl, 2.0 mM NaH_2PO_4, 25.0 mM $NaHCO_3$, 0.5 mM $CaCl_2$, 7 mM $MgCl_2$, 20 mM dextrose, 1.3 mM sodium ascorbate, 0.6 mM sodium pyruvate and 4 mM Kyn. Right hemisphere slices (400 μm thick) were cut in a vibratome and transferred to a chamber containing artificial cerebrospinal fluid (ACSF: 125.0 mM NaCl, 2.5 mM KCl, 2.0 mM NaH_2PO_4, 25.0 mM $NaHCO_3$, 2 mM $CaCl_2$, 1.3 mM $MgCl_2$, 1.3 mM sodium ascorbate, 3.1 mM sodium pyruvate and 10 mM dextrose). Slices were bubbled with 95% O_2 / 5% CO_2 (315 mOsm) and maintained at 30 °C. Recordings were carried out in ACSF at room temperature (25 ± 2 °C) using micro-electrodes (3–5 MΩ) pulled from borosilicate glass (KG-33, Garner Glass). In most experiments, ACSF was supplemented with all-trans retinal (0.1–1 μM, Sigma-Aldrich) to favor ChR2 functionality and 200 μM $BaCl_2$ to increase granule cell excitability by blocking inward rectifier potassium channels[35] (D.A.L. and A.F.S., unpublished observations), thus increasing the number of granule cells activated by light stimuli. The internal solution contained 120 mM potassium gluconate, 20 mM KCl, 5 mM NaCl, 4 mM $MgCl_2$, 0.1 mM EGTA, 10 mM HEPES, 4 mM Tris-ATP, 0.3 mM Tris-GTP, 10 mM phosphocreatine, Alexa Fluor 488 or 594 (5 μg ml^{-1}, Invitrogen), pH 7.3 and 290 mOsm.

Whole-cell recordings (Axopatch 200B, Molecular Devices) were filtered at 2 kHz, digitized (Digidata 1322A, Molecular Devices) and acquired at 20 kHz onto a PC using pClamp 9 (Molecular Devices). In voltage clamp experiments, a holding potential of −80 mV was used for granule cells and −60 or −70 mV for postsynaptic neurons. Action potentials were elicited in current clamp by current steps of 400 ms from 50 to 800 pA in 50-pA increments from a −60-mV baseline membrane potential.

Light stimuli were delivered through the epifluorescence pathway of a Leica DMLFS microscope (100 W Hg lamp, FITC filter cube, 63× water immersion objective, numerical aperture 0.9) and controlled through a UNIBLITZ VMM-D1 shutter (Vincent Associates), commanded from the acquisition software. Slices were briefly scanned for ChR2 expression (GFP or RFP positive) in granule cells and whole-cell patch-clamp recordings were made from neighboring cells in the GCL/hilar border, hilus or pyramidal layer. Light pulses of 10 ms were then delivered at 0.2–4 Hz while we recorded postsynaptic membrane currents in voltage-clamp.

We measured the latency of light-evoked spikes in ChR2-positive neurons from the start of the light pulse to the peak of the action potential. The latency to onset of PSCs was measured from the start of the light pulse to the time when the average PSC reached 10% of the peak amplitude.

Analysis of postsynaptic responses

We estimated the mono-or polysynaptic nature of PSCs using measurements of latency and kinetics combined with pharmacological treatments. A limitation of our approach is that synaptic delays can be estimated, but not measured precisely, as the latency from the light stimulus to the presynaptic spike varies across granule cells according to their ChR2 expression level (Supplementary Fig. 2). When stimulated at 1 Hz with 10-ms light pulses, ChR2-positive neurons spike with latencies of 10–24 ms (median 19.3, $n = 9$). The latencies of monosynaptic PSCs result from adding spike latencies and mossy fiber synaptic delays, which were reported to be ~3–6 ms[36,37]. Some of the light-evoked PSCs (7 out of 14) showed properties that strongly suggest a monosynaptic nature (see examples in Fig. 4a–l): (i) median latency to onset of 17.3 ms (range 14.2–22.0 ms), (ii) fast rise time of average traces (median 1 ms, range 0.7–2.1 ms), also reflecting little jitter in latency[36], and (iii) lack of BMI effect, thus ruling out the possibility of polysynaptic GABAergic signals (Fig. 5c,d). In contrast, in two additional recordings, PSCs showed high latencies (25.0 and 25.6 ms), slow rise times (15.5 and 15.3 ms) and sensitivity to both Kyn and BMI, all evidence of polysynaptic pathways (see examples in Fig. 4m–o and Fig. 5e).

Light-evoked PSCs often had two peaks, separated, on average, by ~12 ms. Individual traces showed that failures could be observed in each component independently (Fig. 4d,h). We propose that both peaks correspond to responses to spike doublets induced in presynaptic granule cells by light stimuli (Supplementary Fig. 2). In fact, in granule cells that responded with more than one spike to 10-ms light pulses, the first two spikes were separated, on average, by ~12 ms. Also, the s.d. of the latency of the second spike was about tenfold higher than that of the first one, thus accounting for the broader appearance of the second PSCs in average traces (Fig. 4e,i). Furthermore, second peaks are not polysynaptic GABAergic signals, as they were insensitive to BMI (Fig. 5c,d).

Statistics and data presentation

The comparison between hilar and CA3 boutons was done using Student's *t* test. All other statistical analyses were carried out with one-way ANOVA followed by Fisher's PLSD *post hoc* analysis when a significant difference was found with ANOVA. All data were presented as means ± s.e.m.

Supplementary Material

Refer to Web version on PubMed Central for supplementary material.

Acknowledgements

We would like to thank J. Jepsen and N. Nashi for technical assistance, S. Herlitze for providing the ChR2 construct, L. Petreanu for helpful discussions, J. Simon for artwork, J. Fiala for providing software and M.L. Gage for helpful suggestions to improve this manuscript. We also acknowledge the support of the Picower Foundation, Lookout Foundation, McDonnell Foundation, US National Institutes of Health grants NS050217 (to F.H.G.) and NS038331 (to C.E.R.), Agencia Nacional de Promoción Científica, Consejo Nacional de Investigaciones Científicas y Técnicas (CONICET), and the Howard Hughes Medical Institute (to A.F.S.). D.A.L. and G.L. were supported by fellowships from CONICET.

References

1. Schinder AF, Gage FH. A hypothesis about the role of adult neurogenesis in hippocampal function. Physiology (Bethesda) 2004;19:253–261. [PubMed: 15381753]
2. Ming GL, Song H. Adult neurogenesis in the mammalian central nervous system. Annu Rev Neurosci 2005;28:223–250. [PubMed: 16022595]
3. Aimone JB, Wiles J, Gage FH. Potential role for adult neurogenesis in the encoding of time in new memories. Nat Neurosci 2006;9:723–727. [PubMed: 16732202]
4. Lledo PM, Alonso M, Grubb MS. Adult neurogenesis and functional plasticity in neuronal circuits. Nat Rev Neurosci 2006;7:179–193. [PubMed: 16495940]
5. Zhao C, Deng W, Gage FH. Mechanisms and functional implications of adult neurogenesis. Cell 2008;132:645–660. [PubMed: 18295581]
6. van Praag H, et al. Functional neurogenesis in the adult hippocampus. Nature 2002;415:1030–1034. [PubMed: 11875571]
7. Schmidt-Hieber C, Jonas P, Bischofberger J. Enhanced synaptic plasticity in newly generated granule cells of the adult hippocampus. Nature 2004;429:184–187. [PubMed: 15107864]
8. Espósito MS, et al. Neuronal differentiation in the adult hippocampus recapitulates embryonic development. J Neurosci 2005;25:10074–10086. [PubMed: 16267214]
9. Ge S, et al. GABA regulates synaptic integration of newly generated neurons in the adult brain. Nature 2006;439:589–593. [PubMed: 16341203]
10. Laplagne DA, et al. Functional convergence of neurons generated in the developing and adult hippocampus. PLoS Biol 2006;4:e409. [PubMed: 17121455]
11. Ge S, Yang CH, Hsu KS, Ming GL, Song H. A critical period for enhanced synaptic plasticity in newly generated neurons of the adult brain. Neuron 2007;54:559–566. [PubMed: 17521569]

12. Toni N, et al. Synapse formation on neurons born in the adult hippocampus. Nat Neurosci 2007;10:727–734. [PubMed: 17486101]
13. Shapiro LA, Upadhyaya P, Ribak CE. Spatiotemporal profile of dendritic outgrowth from newly born granule cells in the adult rat dentate gyrus. Brain Res 2007;1149:30–37. [PubMed: 16904657]
14. Henze DA, Urban NN, Barrionuevo G. The multifarious hippocampal mossy fiber pathway: a review. Neuroscience 2000;98:407–427. [PubMed: 10869836]
15. Zhao C, Teng EM, Summers RG Jr, Ming GL, Gage FH. Distinct morphological stages of dentate granule neuron maturation in the adult mouse hippocampus. J Neurosci 2006;26:3–11. [PubMed: 16399667]
16. Amaral DG. Synaptic extensions from the mossy fibers of the fascia dentata. Anat Embryol (Berl) 1979;155:241–251. [PubMed: 453543]
17. Frotscher M. Mossy fiber synapses on glutamate decarboxylase–immunoreactive neurons: evidence for feed-forward inhibition in the CA3 region of the hippocampus. Exp Brain Res 1989;75:441–445. [PubMed: 2721621]
18. Soriano E, Frotscher M. Spiny nonpyramidal neurons in the CA3 region of the rat hippocampus are glutamate-like immunoreactive and receive convergent mossy fiber input. J Comp Neurol 1993;333:435–448. [PubMed: 8102385]
19. Chicurel ME, Harris KM. Three-dimensional analysis of the structure and composition of CA3 branched dendritic spines and their synaptic relationships with mossy fiber boutons in the rat hippocampus. J Comp Neurol 1992;325:169–182. [PubMed: 1460112]
20. Amaral DG, Ishizuka N, Claiborne B. Neurons, numbers and the hippocampal network. Prog Brain Res 1990;83:1–11. [PubMed: 2203093]
21. Acsady L, Kamondi A, Sik A, Freund T, Buzsaki G. GABAergic cells are the major postsynaptic targets of mossy fibers in the rat hippocampus. J Neurosci 1998;18:3386–3403. [PubMed: 9547246]
22. Boyden ES, Zhang F, Bamberg E, Nagel G, Deisseroth K. Millisecond timescale, genetically targeted optical control of neural activity. Nat Neurosci 2005;8:1263–1268. [PubMed: 16116447]
23. Li X, et al. Fast noninvasive activation and inhibition of neural and network activity by vertebrate rhodopsin and green algae channelrhodopsin. Proc Natl Acad Sci USA 2005;102:17816–17821. [PubMed: 16306259]
24. Walker MC, Ruiz A, Kullmann DM. Monosynaptic GABAergic signaling from dentate to CA3 with a pharmacological and physiological profile typical of mossy fiber synapses. Neuron 2001;29:703–715. [PubMed: 11301029]
25. Gutierrez R. The dual glutamatergic-GABAergic phenotype of hippocampal granule cells. Trends Neurosci 2005;28:297–303. [PubMed: 15927685]
26. Scharfman HE, Kunkel DD, Schwartzkroin PA. Synaptic connections of dentate granule cells and hilar neurons: results of paired intracellular recordings and intracellular horseradish peroxidase injections. Neuroscience 1990;37:693–707. [PubMed: 2247219]
27. Scharfman HE. Evidence from simultaneous intracellular recordings in rat hippocampal slices that area CA3 pyramidal cells innervate dentate hilar mossy cells. J Neurophysiol 1994;72:2167–2180. [PubMed: 7884451]
28. Scharfman HE. Electrophysiological evidence that dentate hilar mossy cells are excitatory and innervate both granule cells and interneurons. J Neurophysiol 1995;74:179–194. [PubMed: 7472322]
29. Kamiya H, Shinozaki H, Yamamoto C. Activation of metabotropic glutamate receptor type 2/3 suppresses transmission at rat hippocampal mossy fiber synapses. J Physiol (Lond) 1996;493:447–455. [PubMed: 8782108]
30. Amaral DG, Dent JA. Development of the mossy fibers of the dentate gyrus. I. A light and electron microscopic study of the mossy fibers and their expansions. J Comp Neurol 1981;195:51–86. [PubMed: 7204652]
31. Seress L, Ribak CE. Postnatal development of CA3 pyramidal neurons and their afferents in the Ammon's horn of rhesus monkeys. Hippocampus 1995;5:217–231. [PubMed: 7550617]
32. Laplagne DA, et al. Similar GABAergic inputs in dentate granule cells born during embryonic and adult neurogenesis. Eur J Neurosci 2007;25:2973–2981. [PubMed: 17509085]
33. Snyder JS, Kee N, Wojtowicz JM. Effects of adult neurogenesis on synaptic plasticity in the rat dentate gyrus. J Neurophysiol 2001;85:2423–2431. [PubMed: 11387388]

34. Campbell RE, et al. A monomeric red fluorescent protein. Proc Natl Acad Sci USA 2002;99:7877–7882. [PubMed: 12060735]

35. Standen NB, Stanfield PR. A potential- and time-dependent blockade of inward rectification in frog skeletal muscle fibres by barium and strontium ions. J Physiol (Lond) 1978;280:169–191. [PubMed: 308537]

36. Jonas P, Major G, Sakmann B. Quantal components of unitary EPSCs at the mossy fiber synapse on CA3 pyramidal cells of rat hippocampus. J Physiol (Lond) 1993;472:615–663. [PubMed: 7908327]

37. Kneisler TB, Dingledine R. Spontaneous and synaptic input from granule cells and the perforant path to dentate basket cells in the rat hippocampus. Hippocampus 1995;5:151–164. [PubMed: 7550611]

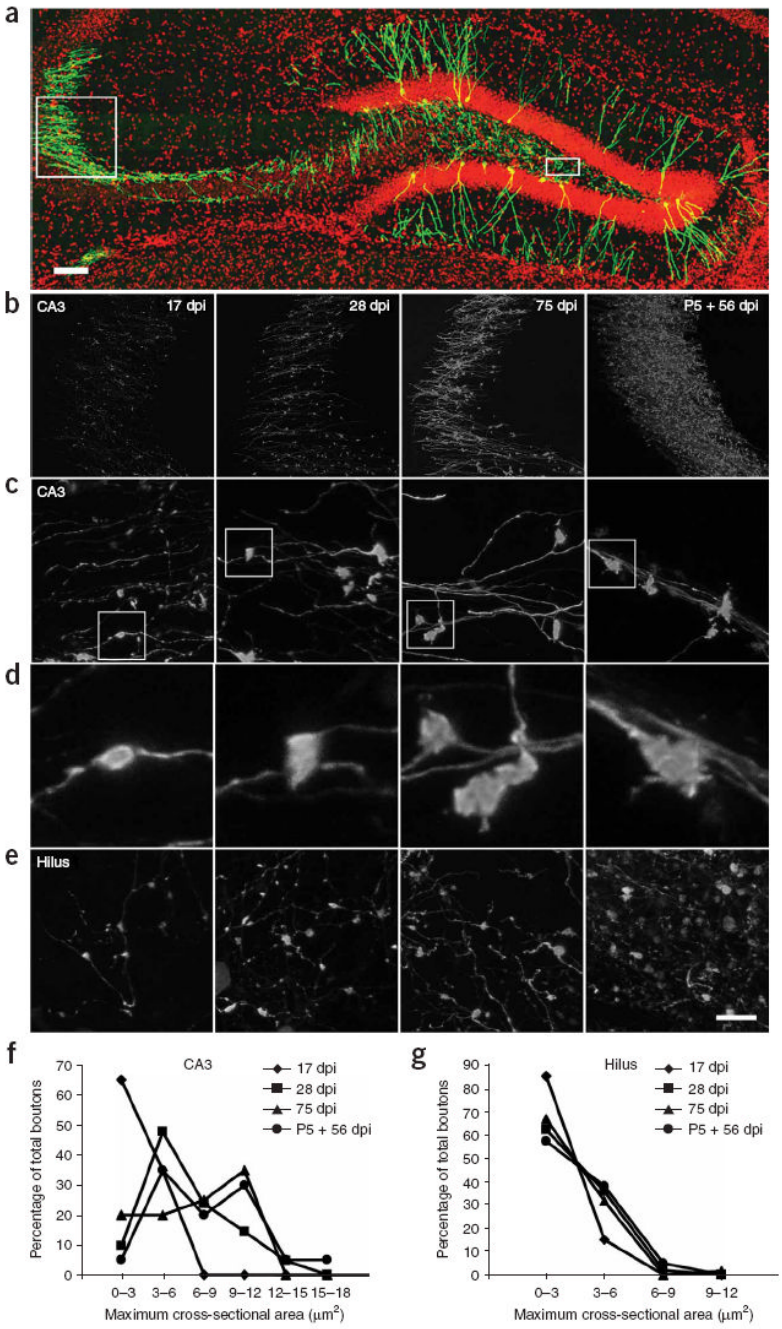

Figure 1. Confocal microscopy of mossy fiber boutons from newborn neurons

(**a**) An overview of the hippocampus with a subpopulation of adult-born neurons in green. Boxed areas indicate the area analyzed in CA3 (left) and the hilus (right). (**b**) Examples of mossy fiber axons labeled with retrovirus at 17, 28 and 75 dpi after virus injection into 6–7-week-old female mice and at 56 dpi after virus injection into a mouse pup at postnatal day 5 (labeled as P5). (**c**) High-magnification views of mossy fiber boutons in CA3. (**d**) Enlarged views of representative boutons that are boxed in **c**. (**e**) High-magnification views of mossy fiber boutons in the hilus. Panels in **c**, **d** and **e** are arranged in the same time point order as **b**. (**f**) Distribution of the size of mossy fiber boutons at different time points in CA3. Mossy fiber boutons were grouped according to their size, and the percentage of boutons in each size group

was quantified. The size of mossy fiber boutons in CA3 was significantly smaller at 17 dpi than at any other time points (t (77) = 10.50, $P < 0.001$, Fisher's PLSD; 17 dpi versus all other time points, $P < 0.002$; 28 dpi versus 75 dpi, $P = 0.42$; 28 dpi versus P5 + 56 dpi, $P = 0.033$; 75 dpi versus P5 + 56 dpi, $P = 0.18$). (**g**) Distribution of the size of mossy fiber boutons at different time points in the hilus. (t (156) = 0.54, $P = 0.65$). Data are presented as means ± s.e.m. Red, DAPI; green, GFP. Scale bars represent 50 μm in **a**, 60 μm in **b**, 10 μm in **c** and **e**, and 2.5 μm in **d**.

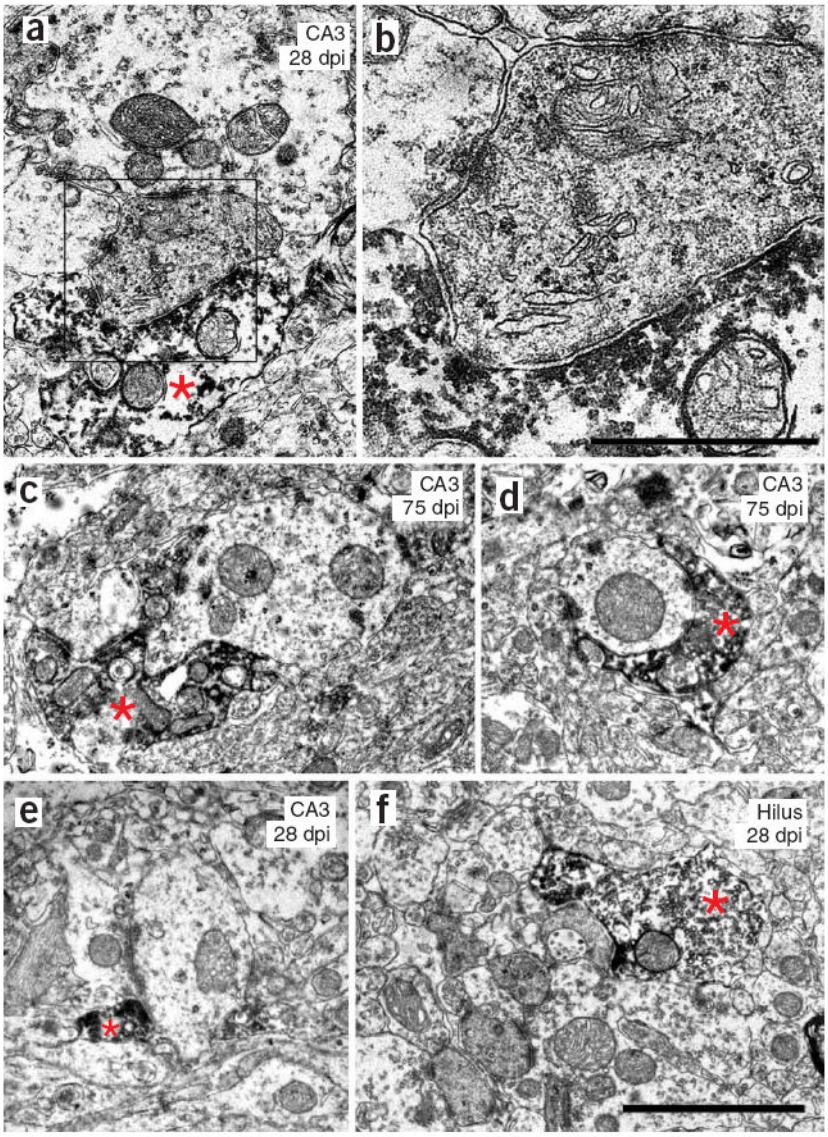

Figure 2. Electron micrographs illustrating the diversity of synapses made by newly generated neurons

(**a**,**b**) GFP-positive mossy terminal synapsing on a thorny excrescence in the CA3 area at 28 dpi The boxed area is enlarged in **b**. (**c**) GFP-positive mossy terminal synapsing on a thin, spiny dendrite in the CA3 at 75 dpi. (**d**) Bouton *en passant* synapsing on a thin, aspiny dendrite in the CA3 area at 75 dpi. (**e**) Bouton *en passant* synapsing on a thin, aspiny dendrite in the CA3 at 28 dpi. (**f**) Mossy terminal synapsing on a thorny excrescence in the hilus at 28 dpi. Scale bars represent 2 μm in **a** and **c**–**f**, and 0.8 μm in **b**. Asterisks indicate GFP-positive axon terminal.

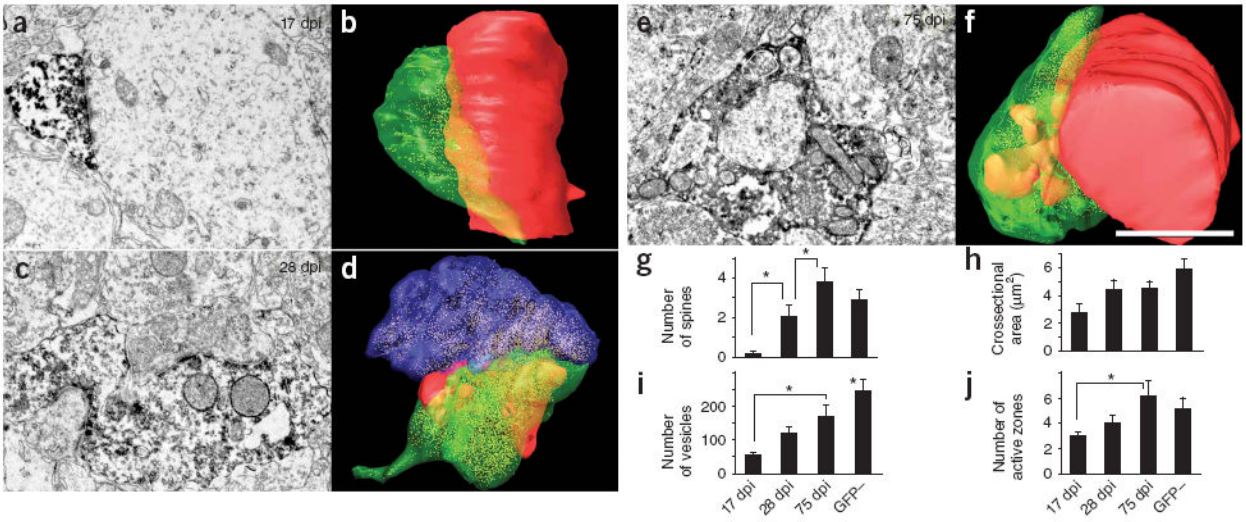

Figure 3. Temporal progression of the morphology of GFP-positive axon terminals in the CA3 area

(**a**,**b**) At 17 dpi, small boutons contacted dendritic shafts. (**c**,**d**) At 28 dpi, GFP-positive larger mossy terminals contacted thorny excrescences that were also contacted by GFP-negative mossy terminals. (**e**,**f**) At 75 dpi, mossy terminals contacted individual thorny excrescences. The boutons shown in the electron micrographs in **a**, **c** and **e** were serially sectioned and three-dimensionally reconstructed in **b**, **d** and **f**. Scale bar represents 1.5 μm. Green, GFP-positive bouton; red, dendrites and spines that synapsed with the GFP-positive boutons; blue, unlabeled axon terminal that shared postsynaptic targets with the GFP-positive bouton. (**g**) Number of spines indenting into GFP-positive boutons, as observed on the largest section. The number at 17 dpi was significantly smaller than at any other time point (t (31) = 6.85, P = 0.01, Fisher's PLSD; 17 versus 28 dpi, P = 0.03; 28 versus 75 dpi, P = 0.03; 75 dpi versus GFP-negative boutons, P = 0.25). (**h**) Cross-sectional area of GFP-positive boutons at the largest section (t (31) = 3.62, P = 0.02). (**i**) Number of presynaptic vesicles in the largest section (t (31) = 7.02, P < 0.001, Fisher's PLSD; 17 versus 75 dpi, P = 0.01; 17 dpi versus GFP-negative, P < 0.001; 28 dpi versus GFP-negative, P < 0.005; 75 dpi versus GFP-negative, P < 0.05). (**j**) Number of active zones in the largest section (t (31) = 2.08, P = 0.12, Fisher's PLSD; 17 versus 75 dpi, P < 0.05). * P < 0.05. Data are presented as means ± s.e.m.

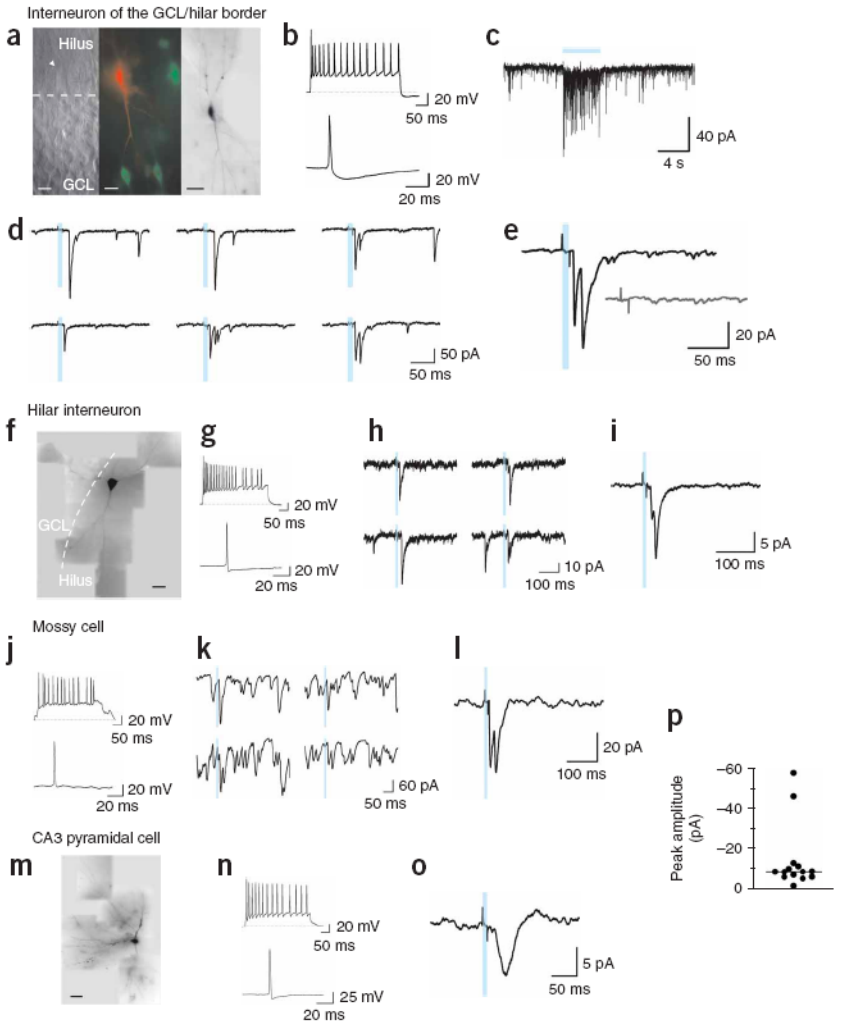

Figure 4. Light-evoked neurotransmitter release from adult-born neurons expressing ChR2

(**a**–**e**) GCL/hilar border interneuron. (**a**) Left, infrared microscopy of a patched neuron (arrowhead). The dashed line divides GCL from hilus. Middle, merged images showing the patched neuron filled with Alexa Fluor 543 (red) and ChR2-GFP-positive granule cells (green). Right, reconstruction of the filled neuron showing bipolar morphology, with dendrites extending toward the GCL and hilus. Scale bars represent 20 μm (left, middle) and 50 μm (right). (**b**) Top, 40-Hz spike train in response to a 750-pA pulse. Bottom, spike elicited by a 50-pA current. (**c**) Synaptic activity evoked by a prolonged light stimulus (blue bar). (**d**) Example PSCs elicited by 10-ms light stimuli (blue bars) delivered at 0.2 Hz. (**e**) Average of 45 responses. PSC delay to onset was 15.2 ms and failure probability of first peak was 0.36. Inset, average of 38 traces evoked with a blocked light path. (**f**–**i**) Hilar interneuron. (**f**) Dye-filled neuron with multipolar morphology and dendrites extending through the hilus and GCL. Scale bar represents 50 μm. (**g**) Top, 50-Hz spike train in response to 700 pA. Bottom, spike elicited by 50 pA. (**h**) Example PSCs. (**i**) Average of 179 responses to repeated stimuli (1 Hz). The PSC delay was 21.9 ms and the failure probability was 0.56. (**j**–**l**) Hilar mossy cell. (**j**) Top, 35-Hz spike train in response to 250 pA. Bottom, spike elicited by 100 pA. (**k**) Example PSCs showing high frequency of spontaneous synaptic activity. (**l**) Average of 445 PSCs (1 Hz). PSC onset was 14.2 ms. (**m**–**o**) CA3 pyramidal cell. (**m**) Filled neuron showing the soma in the CA3 pyramidal layer, with basal and apical dendrites. Scale bar represents 50 μm. (**n**)

Top, 35-Hz spike train in response to 350 pA. Bottom: spike in response to 50 pA. (**o**) Average of 400 PSCs (1 Hz). PSC onset was 25.1 ms. (**p**) Average peak amplitude of all light-evoked PSCs (n = 14 cells). The horizontal line denotes the median.

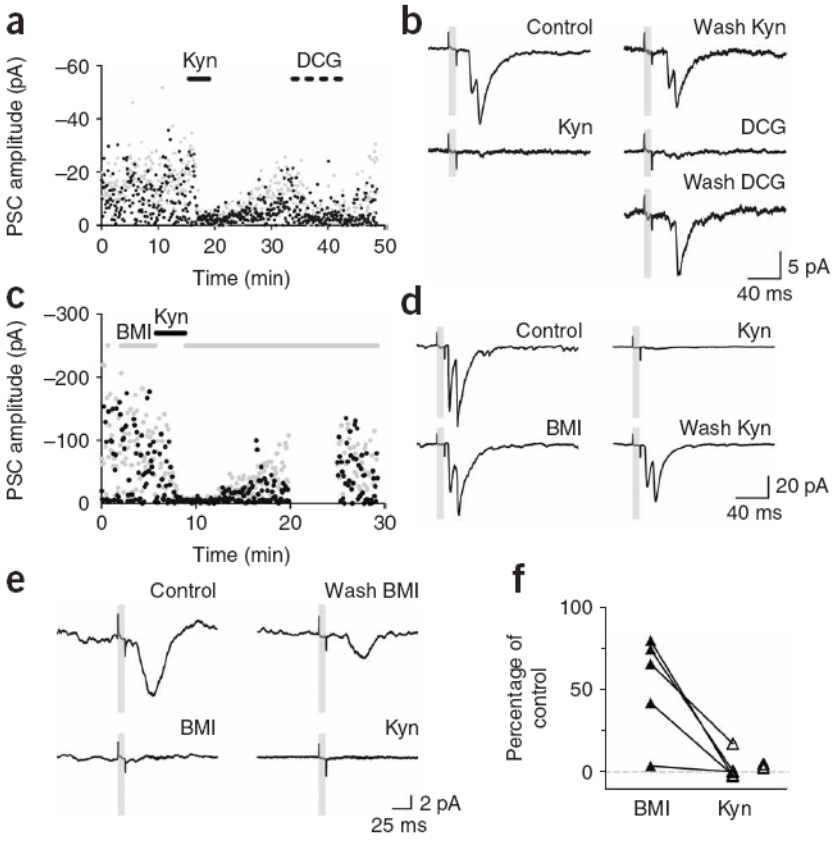

Figure 5. Pharmacological treatments demonstrate glutamate release by adult-born neurons

(**a**) Amplitude of the first and second peak (black and gray dots) of PSCs evoked by repetitive light pulses (0.2 Hz). Application of 10 mM Kyn and DCG-IV (DCG, 1 μM) is indicated by the solid and dotted bars. DCG increased failure probability from 0.27 to 0.85 (same cell as in Fig. 4f–i). (**b**) Consecutive average traces from the experiment shown in **a**, taken before, during or after the indicated treatments. (**c**) Amplitude of the first and second peak of single light-evoked PSCs (0.2-Hz stimulation). Application of 20 μM BMI and 4 mM Kyn is indicated by the gray and black horizontal bars (acquisition was interrupted from 20–25 min; same cell as in Fig. 2a–e). (**d**) Consecutive average traces from the experiment shown in **d**, taken before, during or after the indicated treatments. (**e**) Pharmacology of light-evoked PSCs on a pyramidal cell. Consecutive average traces show a full blockade of PSCs by BMI, partial recovery after drug washout and then full blockade by Kyn. (**f**) Amplitude of light-evoked PSCs in the presence of BMI ($n = 5$) or Kyn ($n = 8$) relative to their amplitude without drugs. Lines connect values obtained in the same neurons. Experiments where BMI was not applied are shown to the right.